Final Draft
of the original manuscript:

He, Y.; Liu, Z.; Zhou, G.; Wang, H.; Bai, C.; Rodney, D.; Appel, F.;
Xu, D.; Yang, R.:

Dislocation dipole-induced strengthening in intermetallic TiAl

In: Scripta Materialia (2017) Elsevier

DOI: 10.1016/j.scriptamat.2017.09.010

Dislocation dipole-induced strengthening in intermetallic TiAl

Yan He[1,2], Zhao Liu[1], Gang Zhou[1,3], Hao Wang[1*], Chunguang Bai[1],
David Rodney[4], Fritz Appel[5], Dongsheng Xu[1], Rui Yang[1]

[1] *Institute of Metal Research, Chinese Academy of Sciences, 110016 Shenyang, China*

[2] *College of Physics and Technology, Shenyang Normal University, 110034 Shenyang, China*

[3] *School of Materials Science and Engineering, Dalian University of Technology, 116024 Dalian, China*

[4] *Institut Lumière Matière, Université Lyon 1, CNRS, UMR 5306, F-69622 Villeurbanne, France*

[5] *Institute for Materials Research, Helmholtz-Zentrum Geesthacht, D-21502 Geesthacht, Germany*

[*] *E-mail: haowang@imr.ac.cn*

Abstract-Narrow dislocation dipoles in intermetallic TiAl are systematically investigated by atomic-scale simulations and electron microscopy. The formation energy of narrow dipolar configurations and the activation energy during their evolution are unraveled. We show that faulted dipoles can be stable over experimental timescales, in full agreement with high-resolution observations. Such stable atomic-scale structures provide a strengthening effect significantly larger than the elastic prediction, which deeply influences plasticity in TiAl.

Keywords: Plasticity; Dislocation; Atomistic simulation; Intermetallics; Faulted dipole

Deformation of γ-TiAl alloys is mainly carried by the glide of ordinary dislocations with the Burgers vector 1/2<110] and a limited amount of mechanical twinning. Superdislocations with <101] and 1/2<11$\bar{2}$] Burgers vectors, which also occur in γ-TiAl, exhibit an asymmetric non-planar core spreading and high glide resistance [1, 2]. The ordinary dislocations have a compact core, which makes cross slip easy. Thus, the screw components of the ordinary dislocations contain a high density of jogs at which dislocation dipoles and debris are trailed and terminated [3. 5]. There is good consensus that this jog dragging mechanism, together with lattice friction (Peierls mechanism), largely determines the mobility of the ordinary dislocations. It has been demonstrated [5] that the jog dragging significantly contributes to strain hardening at ambient temperatures. The stability of dipole structures is important for the evolution of internal stresses [6, 7], dynamic recovery [8] and the temperature retention of strain hardening [5]. Dipole and debris structures were frequently observed in deformed TiAl alloys by transmission electron microscopy (TEM) [5, 9-16]; however, the fine structure of the dipoles and their transformation into point defects is largely unknown. These aspects are addressed in the present study. In this context, we have systematically examined the formation

energy of narrow dipolar configurations and the activation energies during their evolution employing empirical interatomic potentials, covering various dipole heights and orientations. The results are compared with TEM observations in the γ phase of different TiAl alloys. Lastly, the influence on plastic deformation is revealed with dislocation dipole-induced hardening beyond elastic prediction.

Dipole stability was first studied by classical molecular dynamics (MD). Vacancy- and interstitial-type dislocation dipoles in γ-TiAl, with Burgers vectors $\pm 1/2[1\bar{1}0]$, heights 1*d* to 4*d* (*d* is the interplanar distance along [111]) and orientation angles 90°, 74°, 60°, 41° and 30° (defined as the angle between the Burgers vector and the dislocation line), were constructed using the methodology developed in Refs. [3, 4]. Periodic boundary conditions were employed with simulation box dimensions $6[\bar{1}\bar{1}2]$ by $20[1\bar{1}0]$ by 15[111]. Simulations were repeated in larger boxes to ensure negligible influence from the box size. An embedded-atom interatomic potential for the Ti-Al system [17] was employed. Fig. 1 shows the formation energy per vacancy/interstitial of various dipoles under low temperature relaxation. Vacancy dipoles are systematically more energetically stable than interstitial dipoles. Despite certain unexpected behavior of 30° vacancy and interstitial dipoles at 2*d* and 1*d*, respectively, all 60° vacancy dipoles, except at 2*d*, possess the lowest formation energy at any given height. We therefore focus in the following on 60° vacancy dipoles. Their atomic configurations relaxed at 1 K for 50 ps and 1700 K for 1 ns are shown in Fig. 1c1-c4 and d1-d4, respectively. At 1 K, while the 3*d* (Fig. 1c3) and 4*d* (Fig. 1c4) dipoles stabilize as faulted dipoles [14], the 1*d* dipole becomes hollow and the 2*d* dipole is intermediate ,with an open structure showing features of a faulted dipole. At 1700 K, the 3*d* and 4*d* 60°-dipoles remain stable and retain their low-temperature configurations within relaxation times up to 1 ns (Fig. 1d3 and d4), while significant atomic diffusion occurs in 1*d* and 2*d* dipoles (Fig. 1d1 and d2). Atoms are colored according to their coordination number (Fig. 1c1-c4) or FCC-coordination number (Fig. 1d1-d4) using AtomEye [18].

Such high stability of the 3*d* and 4*d* dipoles coincides with experimental observations of wide and narrow faulted dipoles under TEM (Fig. 2a, also see Fig. 5 in Ref. [14]) and high resolution TEM (Fig. 2b) [5], respectively.

A characteristic feature is a dense structure of dislocation dipoles with a size distribution varying from 200 nm down to vanishingly small loops, which are referred to collectively as debris. The origin of a dipole is often traceable back to ordinary dislocations, which suggests that it was trailed and terminated at jogged screw dislocation. The dipoles are almost perpen-

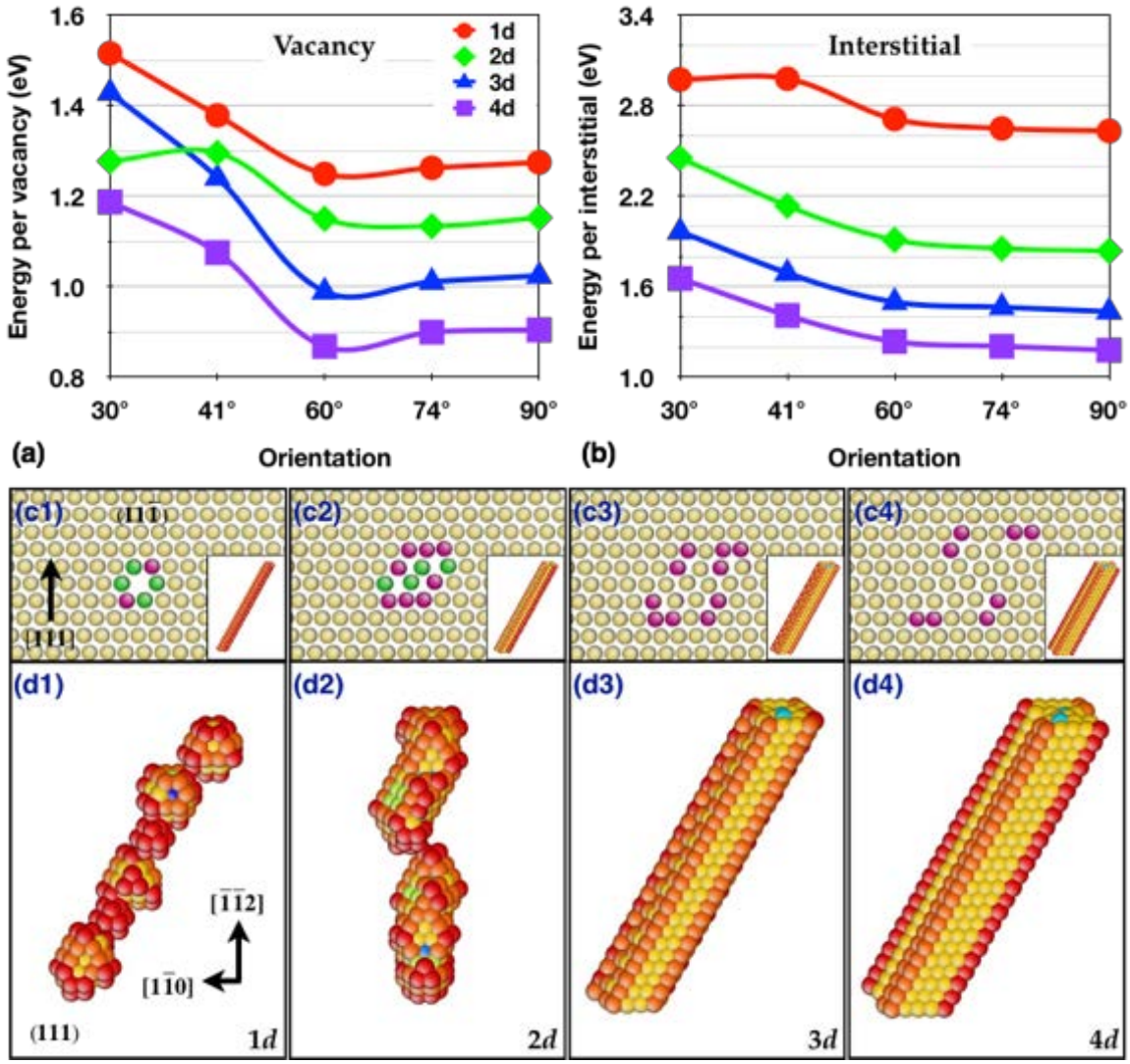

Fig. 1 (a/b) Formation energy per vacancy/interstitial of dipoles of various heights and orientations. Note the local minima at 60°. (c-d) Atomic configurations of 60° dipoles with heights 1*d* to 4*d* relaxed at 1 K for 50 ps (c1-c4) and at 1700 K for 1 ns (d1-d4). Atoms are colored according to their coordination number (c1-c4) or FCC-coordination number (d1-d4). Lattice orientations are indicated.

dicularly elongated with respect to the Burgers vector, i.e., the two dipole arms have edge character and are situated on parallel glide planes. The detailed configuration depends on the height of the jog from which the dipole was trailed. At a sufficiently high stress, a screw dislocation may drag a mono-atomic jog along, which will leave behind a trail of vacancies or

interstitial atoms depending on the sign of the dislocation and the direction the dislocation is moving. At taller jogs, dislocation dipoles are trailed as the screw dislocation moves, i.e., the jog is connected to the moving dislocation by two lengths of edge dislocations of opposite sign. Because of the mutual attraction of the positive and negative edge dislocations forming the dipole, a dipole may break up in a row of prismatic loops. Widely separated dipole arms may overcome their elastic interaction and operate as single-ended dislocation sources, for details see [5]. As an example, Fig. 2a shows the structure of dislocation produced during low cycle fatigue at T=550°C. The micrograph shows numerous dipoles of different heights; high dipoles are about to open under combined glide and climb forces. Arrow (1) indicates an ordinary 1/2<110] screw dislocation trailing a 90° dipole, and arrow (2) designates dislocation dipoles that act as single ended dislocation sources. The orientation of the Burgers vector is noted as "b". Fig. 2b shows a small dislocation dipole produced during room temperature compression with its two edge dislocation arms under high resolution TEM along the $<10\bar{1}]$ direction (Appel *et al*. [5]). The dipole has vacancy character because the (111) slip planes of the unlike edge dislocations are separated by a few atomic spacing, with the extra half planes lying outside the dipole. Here the MD result agrees well with the experimental observation. Fig. 2c shows the MD-predicted 3*d* 60° dipole as in Fig. 1c3, but reoriented according to the TEM image of Fig. 2b. For comparison, Fig. 1c3 is recalled in the inset, but rotated. The result indicates that the experimentally observed dipole in Fig. 2b is a vacancy dipole with a height of 3*d* and an orientation of 60°.

The long-term stability of 60° dipoles was predicted by searching for thermally-activated transitions (Fig. 3a) with the activation-relaxation technique (ART) [19, 20] and the lowest-energy path (Fig. 3b) with the autonomous basin climbing (ABC) method [21, 22]. In each ART calculation, a total of 2000 trials were performed, starting from the same initial configuration. For each trial, an atom was chosen randomly among the high-energy atoms (with excess energy between 0.1 eV and 1.0 eV) and was activated together with its neighbors within 5 Å. In ABC calculations, Gaussian potentials were added to the most energetic atoms (with excess energy between 0.1 eV and 1.0 eV) with Gaussian height and width of 0.05 eV and 0.6 Å, respectively. The above choices in ART and ABC simulations are based on the experience we have gained in metallic systems and also for computation efficiency (for details, please refer to Ref. [4, 23]). For 1*d* and 2*d* dipoles, both ART and ABC calculations successfully discovered low-energy transitions (circles and diamonds in Fig. 3a, and red and green lines in Fig. 3b) leading to a segmentation of the dipoles, as in Fig. 1d1 and 1d2. However, for 3*d* and

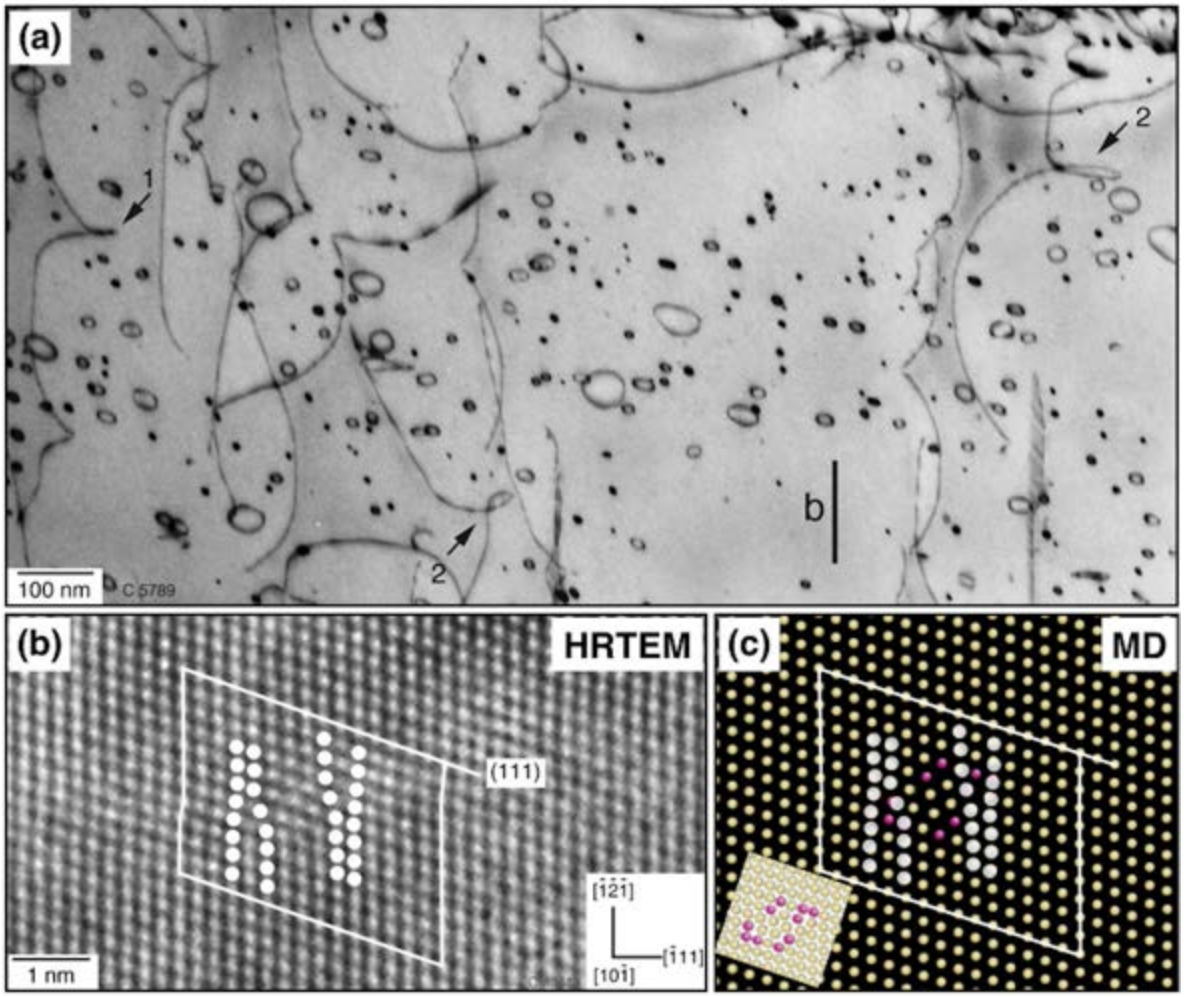

Fig. 2 Dislocation dipoles in γ-TiAl. (a) Structure of dislocation dipoles produced during low cycle fatigue at T=550°C under strain control with a total strain amplitude $\Delta\varepsilon_t/2$=0.7% and a total number of N_f=452 cycles. Extruded, nearly lamellar Ti-45Al-8Nb-0.2C (at. %), TNB-V2. The micrograph shows numerous dipoles of different heights. High dipoles are about to open under combined glide and climb forces. Arrow (1) indicates an ordinary 1/2<110] screw dislocation trailing a dipole, arrow (2) designates dislocation dipoles that act as single ended dislocation sources. b indicates the orientation of the Burgers vector. (b) High resolution image along the <10$\bar{1}$] direction, showing a small dislocation dipole across its two edge dislocation arms. The (111) slip planes of the unlike edge dislocations are separated by a few atomic spacings, indicating the vacancy character of the dipole. The total projected Burgers vector of the dipole configuration is zero, as indicated by the Burgers circuit. Ti-48Al-2Cr (at. %) (Appel et al. [5], micrograph reused with permission of Elsevier). (c) The simulated atomic configuration after MD annealing projected along the 60° orientation (the same as Fig. 1c3 as indicated by the inset).

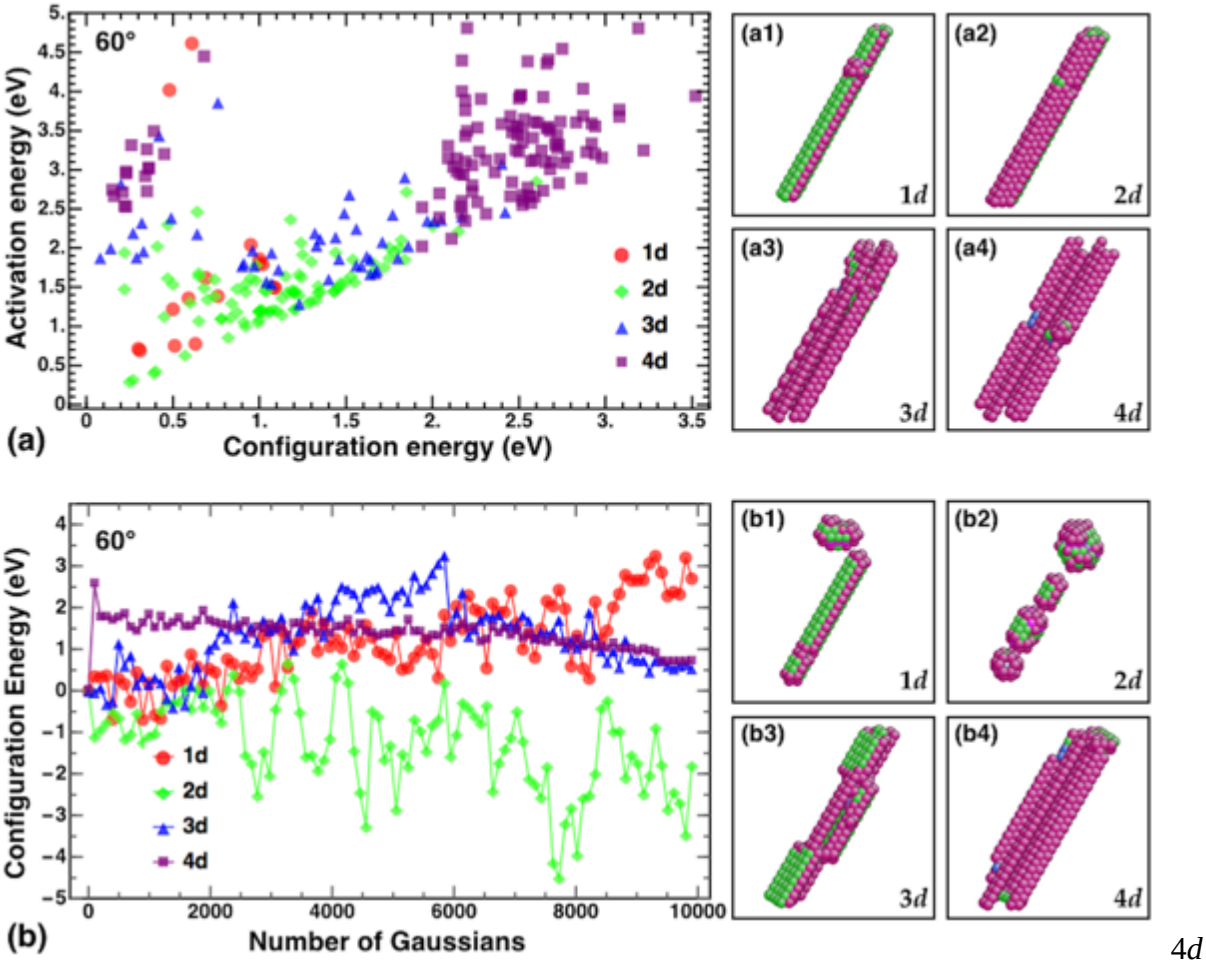

Fig. 3 Energy profiles and atomic configurations during the long-term evolution of 60° dipoles of heights 1*d* to 4*d*. (a) Activation energies of the first transitions calculated by ART. (a1-a4) Configurations after the lowest-energy first transitions in (a). (b) Lowest-energy paths calculated by ABC. (b1-b4) Configurations after adding 10000 Gaussians as shown in (b).

dipoles, ART did not find any energy barrier below 1.0 eV (triangles and squares in Fig. 3a) and the paths found by ABC correspond to the migration of the dipoles rather than their disintegration (Fig. 3b3 and 3b4). These results are consistent with the MD prediction, and confirm the stability of 60° dipoles higher than 2*d*.

Dipole stability has various implications on plasticity. On the modeling side, dipole stability must be considered in recovery models [5], as dislocations often rearrange into dipole configurations with lower energy before annihilation eventually occurs. Also affected is the concept of passing stress [6] used to evaluate the back stress provided by dipolar dislocations.

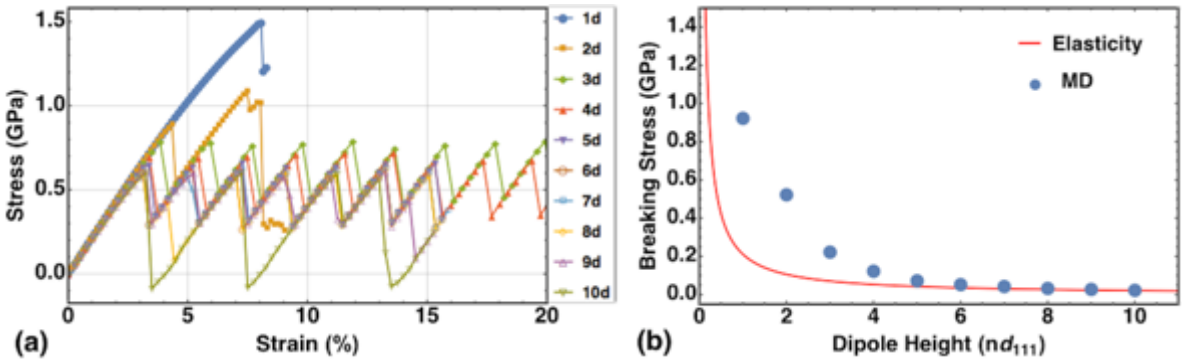

Fig. 4 (a) Stress-strain curves of the 60° dipolar configurations with heights up to 10*d* (e.g., 1*d* to 4*d* dipoles in Fig. 1c1-c4) under shear loading at 10^7/s and 300 K. (b) The stress necessary to separate a dislocation dipole against dipole height predicted by the elastic theory (solid line) and calculated by MD (filled circles).

For this task, we evaluated the strength of dipolar configurations by applying a shear stress along the glide planes of the constituent dislocations. The stress necessary to separate a dipole, i.e., the breaking stress, increases as the dipole height decreases (Fig. 4a). Compared with the elastic estimation (passing stress, detailed calculation can be found in Ref. [24]), the breaking stress is significantly increased due to the stability of the narrow dipoles (Fig. 4b), implying enhanced contribution of dipoles to the back stress. Veyssière and Chiu [6] have pointed out that the dislocation dissociation into partials has a far larger influence than the elastic anisotropy, which is the main reason of the disagreement between MD and elasticity. Also in Fig. 4b, we subtracted the background stress contribution of TiAl alloys with composition close to Ti-50Al (see Table 3 of Ref. [25]). On the practical side, the present study not only helps to clarify the profuse and puzzling existence of dipoles [5, 9-16], especially of faulted dipoles in deformed γ-TiAl, but also prove their role in dislocation organization [26].

In summary, narrow dislocation dipoles in γ-TiAl were systematically investigated with atomistic simulations and high-resolution experiments. The formation energy of narrow dipolar configurations and the activation energy during their evolution were determined. The results indicate the preference of vacancy dipole against interstitial dipoles, especially the stability of 60º faulted dipoles over other forms on the experimental timescale. The atomic-scale structure and long-term stability of faulted dipoles are in full agreement with high-resolution and ordinary TEM observations. The strengthening effect induced by stable narrow dipoles is significantly larger than elastic predictions, showing that the dipolar contribution to the back stress has so far been underestimated in plasticity models of TiAl.

This work is supported by the National Key Research and Development Program of China (2016YFB0701304, 2016YFB0701305), the Natural Science Foundation of China (51671195) and the Youth Innovation Promotion Association of Chinese Academy of Sciences (2015151). HW is grateful to Dr. Patrick Veyssière (1947-2011) for fruitful discussions. Simulations were performed in the CAS-Shenyang Supercomputing Center.

References

[1] M.H. Yoo, C.L. Fu, Metall Mater Trans A, 1998;29:49-63.

[2] H.N. Wu, D.S. Xu, H. Wang, R. Yang, J. Mater. Sci. Technol. 32 (2016) 1033.

[3] H. Wang, D.S. Xu, R. Yang, P. Veyssière, Acta Mater, 2009;57:3725-3737.

[4] H. Wang, D.S. Xu, D. Rodney, P. Veyssière, R. Yang, Model Simul Mater Sci Eng, 2013;21:025002.

[5] F. Appel, D. Herrmann, F.D. Fischer, J. Svoboda, E. Kozeschnik, Int J Plasticity, 2013;42:83-100.

[6] P. Veyssière, Y.L. Chiu, Philos Mag, 2007;87:3351-3372.

[7] R. Hoppe, F. Appel, Acta Mater, 2014;64:169-178.

[8] U. Essmann, H. Mughrabi, Philos Mag A, 1979;40:731-756.

[9] Y.G. Zhang, Q. Xu, H.X. Li, Scripta Metall Mater, 1992;26:865-870.

[10] B. Viguier, K.J. Hemker, R. Schaublin, J.L. Martin, J Phys IV, 1993;3:441-444.

[11] Q. Xu, Y.G. Zhang, I.P. Jones, C.Q. Chen, Scripta Metall Mater, 1995;32:225-228.

[12] Y. Gao, J. Zhu, Q.G. Cai, The observation on faulted dipoles in deformed TiAl-based alloys, in: J.A. Horton, I. Baker, S. Hanada, R.D. Noebe, D.S. Schwartz (Eds.) High-Temperature Ordered Intermetallic Alloys VI, Materials Research Society, Pittsbugh, PA, 1995, pp. 617-622.

[13] B. Viguier, K.J. Hemker, Philos Mag A, 1996;73:575-599.

[14] F. Grégori, P. Veyssière, Philos Mag A, 2000;80:2933-2955.

[15] Y.L. Chiu, H. Inui, T. Nakano, P. Veyssière, Philos Mag Lett, 2003;83:485-493.

[16] Y.L. Chiu, F. Gregori, T. Nakano, Y. Umakoshi, P. Veyssière, Philos Mag, 2003;83:1347-1363.

[17] R.R. Zope, Y. Mishin, Phys Rev B, 2003;68:024102.

[18] J. Li, Model Simul Mater Sci Eng, 2003;11:173-177.

[19] N. Mousseau, G.T. Barkema, Phys Rev E, 1998;57:2419-2424.

[20] R. Malek, N. Mousseau, Phys Rev E, 2000;62:7723.

[21] A. Kushima, X. Lin, J. Li, J. Eapen, J.C. Mauro, X.F. Qian, P. Diep, S. Yip, J Chem Phys, 2009;130:224504.

[22] Y. Fan, A. Kushima, B. Yildiz, Phys Rev B, 2010;81:104102.

[23] H. Wang, D. Rodney, D.S. Xu, R. Yang, P. Veyssière, Philos Mag, 2013;93:186-202.

[24] H. Wang, D.S. Xu, R. Yang, P. Veyssière, Acta Mater, 2008;56:4608-4620.

[25] F. Appel, R. Wagner, Mater Sci Eng R, 1998;22:187-268.

[26] P. Veyssière, H. Wang, D.S. Xu, Y.L. Chiu, IOP Conf Series: Mater Sci Eng, 2008;3:012018.